# Absence of long-range superconducting correlations in the frustrated half-filled-band Hubbard model

S. Dayal, R. T. Clay, and S. Mazumdar

# Absence of long-range superconducting correlations in the frustrated $\frac{1}{2}$-filled band Hubbard model

S. Dayal,[1] R.T. Clay,[1] and S. Mazumdar[2]

[1]*Department of Physics and Astronomy and HPC*[2] *Center for Computational Sciences,*
*Mississippi State University, Mississippi State, MS, 39762*
[2]*Department of Physics, University of Arizona, Tucson, AZ, 85721*

We present many-body calculations of superconducting pair-pair correlations in the ground state of the half-filled band Hubbard model on large anisotropic triangular lattices. Our calculations cover nearly the complete range of anisotropies between the square and isotropic triangular lattice limits. We find that the superconducting pair-pair correlations decrease monotonically with increasing onsite Hubbard interaction $U$ for inter-pair distances greater than nearest neighbor. For the large lattices of interest here the distance dependence of the correlations approaches that for noninteracting electrons. Both these results are consistent with the absence of superconductivity in this model in the thermodynamic limit. We conclude that the effective $\frac{1}{2}$-filled band Hubbard model, suggested by many authors to be appropriate for the $\kappa$-(BEDT-TTF)-based organic charge-transfer solids, does not explain the superconducting transition in these materials.

## I. INTRODUCTION

The two dimensional (2D) Hubbard model has been extensively investigated because at $\frac{1}{2}$-filling it can successfully describe the antiferromagnetic (AFM) phases found in many strongly-correlated materials. Since AFM phases often occur in materials displaying unconventional superconductivity (SC), such as the high-$T_c$ cuprates and the organic $\kappa$-(BEDT-TTF)$_2$X (hereafter $\kappa$-(ET)$_2$X) charge transfer solid (CTS) superconductors, it has frequently been suggested that some small modification of the model can yield a superconducting state where the residual AFM fluctuations mediate an attractive pairing interaction. In the case of the cuprates, this modification involves a change in the carrier concentration ("doping"); the doped 2D Hubbard model has been intensively investigated with numerous analytic and numerical methods, but whether or not SC occurs within this model is still controversial.

The AFM state in the 2D Hubbard model can also be destroyed at fixed carrier concentration by the introduction of lattice frustration. The model on the anisotropic triangular lattice (see Fig. 1) has been used to describe the $\kappa$-(ET)$_2$X family of CTS, where SC occurs at fixed carrier density under application of moderate pressure. The ET layers here consist of strongly dimerized anisotropic triangular lattices, with the intradimer hopping integrals much larger than the interdimer ones. Each $(ET)_2^+$ dimer contains one hole carrier on the average. This has been used to justify replacing each dimer unit cell with a single site, and the underlying $\frac{1}{4}$-filled cation band with an *effective* $\frac{1}{2}$-filled band[1].

We investigate ground state superconducting pair-pair correlations within the Hamiltonian,

$$
\begin{aligned}
H = & -t \sum_{\langle ij \rangle, \sigma} (c_{i,\sigma}^\dagger c_{j,\sigma} + H.c.) - t' \sum_{[kl], \sigma} (c_{k,\sigma}^\dagger c_{l,\sigma} + H.c.) \\
& + U \sum_i n_{i,\uparrow} n_{i,\downarrow}.
\end{aligned} \tag{1}
$$

In Eq. 1, $c_{i,\sigma}^\dagger$ creates an electron of spin $\sigma$ on site $i$ and $n_{i,\sigma} = c_{i,\sigma}^\dagger c_{i,\sigma}$. $U$ is the on-site Hubbard interaction. We consider a square lattice with hopping integral $t$ along $x$ and $y$-directions and frustrating hopping $t'$ along the $x + y$-direction (see Fig. 1). The limits $t'/t = 0$ and 1 correspond to the square and the isotropic triangular lattices, respectively. All quantities with dimensions of energy will be expressed hereafter in units of $t$. We consider only the $\frac{1}{2}$-filled band corresponding to an electron density per site $\rho = 1$.

The non-superconducting phases of this model, shown schematically in Fig. 1, are relatively well established. As $t'$ is increased in strength, frustration destroys the $\mathbf{q}=(\pi,\pi)$ AFM ground state, replacing it with either a paramagnetic metallic (PM) state or a non-magnetic insulator (NMI) state[2,3]. Numerical calculations on this model and the related model with two diagonal $t'$ bonds in each plaquette have confirmed the presence of the PM, AFM, and NMI phases[2–19]. The NMI phase has been suggested as a candidate state[3] that explains the apparent quantum spin liquid (QSL) behavior seen in the strongly frustrated $\kappa$-(ET)$_2$Cu$_2$(CN)$_3$[1]. As the NMI phase has already been extensively investigated[3,4,6,9,15,16], in the present work we will not consider the properties of this phase any further, but will rather focus on the possibility of SC within the model.
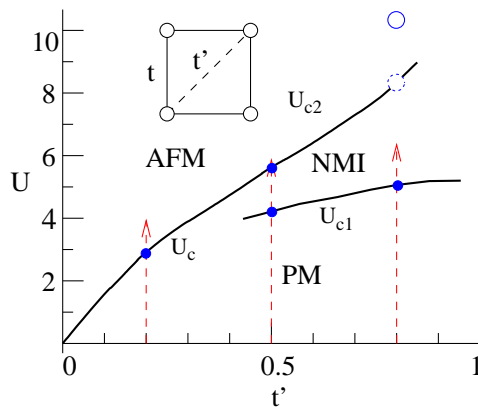
FIG. 1: (color online) Lattice structure (see inset) and the ground state phase diagram of the $\frac{1}{2}$-filled band Hubbard model on the anisotropic triangular lattice for $0 \leq t' < 1$. Phases labeled are paramagnetic metallic (PM), Néel antiferromagnetic (AFM), and non-magnetic insulator (NMI). $d_{x^2-y^2}$ superconductivity has been suggested to occur near the boundary of the AFM and PM phases (see text). Filled circles are finite-size scaled values for phase boundaries from PIRG calculations (see Section IV). The precise value of $U_{c2}$ at $t' = 0.8$ is known with less certainty. At $t' = 0.8$ the solid circle is an exact upper bound from the 4×4 lattice, while the dashed circle shows the expected finite-size scaled value. The phase boundary lines linking the points are only schematic guides to the eye. Dashed vertical lines indicate the parameter regions we investigate for superconductivity.

Numerous mean-field theories have suggested that unconventional SC occurs adjacent to AFM-PM phase boundaries[7,8,20–26]. Similar superconducting states have been suggested for the closely related Hubbard-Heisenberg model on the same lattice[27–31]. Because of the proximity of $(\pi,\pi)$ AFM order, the suggested symmetry of the SC order parameter is $d_{x^2-y^2}$. For $t' \sim 1$ the magnetic ordering $\mathbf{q}$ shifts to $(\frac{2\pi}{3},\frac{2\pi}{3})$ corresponding to the 120° ordering found in the triangular lattice antiferromagnetic Heisenberg model, and consequently superconducting other order parameter symmetries have been suggested[30]. The estimated value of $t'$ for the $\kappa$-ET materials is however smaller than 1 (see below)[32,33], and also no evidence for 120° AFM order is found experimentally within the $\kappa$-ET family[1].

Superconducting pair-pair correlations calculated with numerical methods going beyond mean field theory provide a more accurate assessment of the presence of SC, provided finite-size effects can be adequately controlled. Two criteria must be satisfied to confirm SC within the model: (i) the superconducting pair-pair correlations must be enhanced over the $U = 0$ values over at least a range of $U$, and (ii) the pair-pair correlations must extrapolate to a finite value at long inter-pair distances. We have previously calculated pair-pair correlations for the 4×4 lattice using exact diagonalization[10]. No enhancement of the pair-pair correlations by $U$ was found in these calculations, except for a trivial short-distance enhancement[10] (see also below). Our present work allows more careful analyses of the distance dependence of the pair-pair correlations, as well as the U-dependence of the longer-range components of these correlations, that were not possible within the earlier small cluster calculation.

Pair-pair correlations for lattices comparable to those in the present work have also been calculated using variational quantum Monte Carlo (VMC) methods[13,15,17,34,35]. VMC results however depend to a great degree on the choice of the variational wavefunction, and there is considerable differences of opinion within the existing VMC literature. Clearly, studies of pair-pair correlations on large lattices, using many-body methods that do not depend on an a priori choice of the wavefunction are desirable. A candidate method for calculations of strongly-correlated systems is the recently developed Path Integral Renormalization Group (PIRG) method[36–39]. Like VMC, PIRG is also variational and does not suffer from a fermion sign problem as do standard quantum Monte Carlo methods. Unlike VMC methods however, instead of an assumed functional form of the wavefunction, PIRG uses an *unconstrained* sum of Slater determinants that is optimized using a renormalization procedure[36–39]. The NMI phase within Eq. 1 was first identified using PIRG[2,3]. Previous PIRG calculations[2–4,6,16] investigated the metal-insulator transition, AFM ordering, and properties of the NMI phase in detail, but did not discuss superconducting pair-pair correlations. Here we revisit the model with PIRG and calculate pair-pair correlations as a function of $t'$ and $U$. As explained in Section III, we use the most accurate version of the PIRG ground-state method, Quantum Projection-PIRG (QP-PIRG), which combines symmetries with the renormalization procedure[38]. As explained in Section III, we also performed an "annealing" procedure to help prevent the method from converging to local minima.

While early tight-binding bandstructures calculated using the extended Hückel method found some $\kappa$-ET superconductors to have nearly isotropic triangular lattices with $t' \approx 1$, recent ab-initio methods have determined that $t'$ in the experimental systems lie within the range $0.4 \lesssim t' \lesssim 0.8$[32,33]. Importantly, in this range of anisotropy the 120° AFM order is not relevant. Furthermore, the AFM order is known experimentally to be of the conventional Néel

pattern[40,41]. Consequently, we limit our calculations to $t' \lesssim 0.8$. Specifically, we perform our calculations for three distinct $t' = 0.2$, $0.5$, and $0.8$, as shown in Fig. 1. The two large $t'$ values chosen bracket the estimated frustration in the $\kappa$-ET superconductors[32,33]. We choose a smaller $t' = 0.2$ in addition because it has been suggested in some studies that SC is present even in the weakly frustrated region of the phase diagram[17,26,30]. The phase diagram (Fig. 1) is qualitatively different at $t' = 0.2$ because the NMI phase does not occur for $t' < 0.5$[2,3,6]. While the estimate for degree of frustration is remarkably consistent between different ab-inito methods[32,33], the estimated value of $U$ for $\kappa$-$(ET)_2 X$ is less certain. We therefore perform our calculations over a range of $U$ starting from $U = 0$.

The organization of the paper is as follows. In Section II, we introduce definitions of the order parameters we calculate. In Section III we describe the PIRG method. Section IV presents our data for $t' = 0.2$, $0.5$, and $0.8$, followed by discussions and conclusion in Section V.

## II.   ORDER PARAMETERS

To determine whether SC is present near the metal-insulator (MI) transition, in addition to superconducting correlations we need order parameters to distinguish between metallic and insulating phases. To locate the MI transition we use two different quantities. The first is the double occupancy $D = \langle n_{i\uparrow} n_{i\downarrow} \rangle$. As $U$ increases, a discontinuous decrease in $D$ occurs at the MI transition[3]. In addition, we calculate the bond order $B_{ij}$ between sites $i$ and $j$,

$$B_{ij} = \sum_\sigma \langle c^\dagger_{i,\sigma} c_{j,\sigma} + H.c. \rangle. \tag{2}$$

In the following we have labeled the bond order between sites linked by the $t'$ bond as $B'$. This particular bond order is nonzero in the PM phase but tends to zero in the AFM Néel ordered phase because there electrons on sites connected by $t'$ have parallel spin projections[10].

The operator $\Delta^\dagger_{i,j}$ creates a singlet pair on lattice sites $i$ and $j$:

$$\Delta^\dagger_{i,j} = \frac{1}{\sqrt{2}} (c^\dagger_{i,\uparrow} c^\dagger_{j,\downarrow} - c^\dagger_{i,\downarrow} c^\dagger_{j,\uparrow}). \tag{3}$$

The pair-pair correlation function is defined as

$$P_\alpha(\mathbf{r}) = \frac{1}{4} \sum_\nu g(\nu) \langle \Delta^\dagger_i \Delta_{i+\mathbf{r}(\nu)} \rangle. \tag{4}$$

In Eq. 4 the phase factor $g(\nu)$ determines the symmetry of the superconducting order parameter. We consider two possible pairing symmetries, $d_{x^2-y^2}$ pairing ($\alpha = d$ in our nomenclature below) where $g(\nu) = \{+1, -1, +1, -1\}$ and $\mathbf{r}(\nu) = \{\hat{x}, \hat{y}, -\hat{x}, -\hat{y}\}$, and $d_{xy}$ pairing ($\alpha = xy$) where $g(\nu) = \{+1, -1, +1, -1\}$ and $\mathbf{r}(\nu) = \{\hat{x}+\hat{y}, -\hat{x}+\hat{y}, -\hat{x}-\hat{y}, \hat{x}-\hat{y}\}$.

In the presence of superconducting long-range order, $P_\alpha(\mathbf{r})$ for the ground state in the appropriate pairing channel must converge to a nonzero value for $|\mathbf{r}| \to \infty$. This is seen clearly for example in the 2D $-U$ Hubbard model[42–44]. In the thermodynamic limit the long-distance limit of the pair-pair correlation function, $P_\alpha(r \to \infty)$, is proportional[45] to the square of the superconducting order parameter, $\langle \Delta_\alpha \rangle^2 \propto |P(_\alpha(r \to \infty)|$. The magnitude of $\langle \Delta_\alpha \rangle$ may further be used to set limits[45] on the superconducting condensation energy, gap amplitude, and $T_c$.

## III.   METHOD

The PIRG method has been previously used for a variety of strongly-correlated systems including the 2D Hubbard model[37], $\frac{1}{2}$-filled frustrated 2D Hubbard models[2,3,6,16,38], and the $\frac{1}{2}$-filled Hubbard model on the checkerboard lattice[46,47]. Details of the method are well described in these references. Here we discuss details of our PIRG implementation, and present comparisons with exact results which demonstrate the accuracy of the method for calculating pair-pair correlations.

The PIRG method uses a basis of $L$ Slater determinants, $|\phi_i\rangle$. For $L = 1$ this coincides with the Hartree-Fock (HF) approximation. In practical calculations, maximum $L$'s of a few hundred are used. The method is initialized with the $L = 1$ HF wavefunction or a similar random starting wavefunction, and the PIRG renormalization procedure[37] is used to minimize the energy by optimizing through the action of the operator $\exp(-\tau H)$. One potential problem with the PIRG renormalization procedure is that the method can become trapped in a local minimum and not reach the true ground state[46]. Yoshioka et al. introduced a technique for avoiding local trapping by introducing global
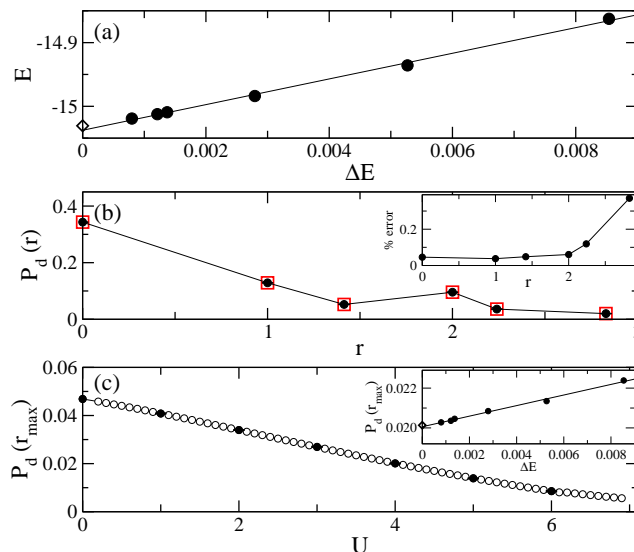
FIG. 2: (color online) Comparison of PIRG and exact results for the 4×4 lattice with $t' = 0.5$. (a) Variance extrapolation of the ground state energy for $U = 4$. The symbol at $\Delta E=0$ is the exact energy; the line is a linear fit. (b) $P_d(r)$ versus $r$. Open (filled) symbols are exact (PIRG) results. The inset shows relative percent error in $P_d(r)$ as a function of $r$. (c) $P_d(r)$ at the largest possible pair spacing on the finite lattice, $P_d(r_{\max})$, as a function of $U$. Open (filled) symbols are exact (PIRG) results. The inset shows the variance extrapolation of $P_d(r_{\max})$ for $U = 4$.

modifications to the wavefunction[46]. Following Ref. 46, we also introduced similar global modifications of the PIRG wavefunctions ("iteration A" in Ref. 46), which modify determinants in a global manner by acting on the wavefunction with $\exp[-\tau H]$ defined by a *random* set of Hubbard-Stratonovich variables. In addition, we also introduced updates to the $|\phi_i\rangle$ based on adding a random variation to the matrix elements of $[\phi_i]_{j,k}$. The amplitude of the variations is decreased systematically in a manner similar to simulated annealing. We found the addition of these two global updates to significantly improve the accuracy of the results.

We also incorporated lattice and spin-parity symmetries in the calculation[38]. Reference 38 introduced two different methods of using symmetry projection: (i) PIRG-QP, where symmetry projectors are applied to the ground state wavefunction after it has optimized using PIRG; and (ii) QP-PIRG, where symmetry projectors are applied at each step of the PIRG optimization. Here we have used the second more accurate of these two approaches, QP-PIRG. The lattice symmetries we used included translation, inversion, and mirror-plane symmetries, a total of $4N$ symmetries where $N$ is the number of lattice sites. We also applied the spin-parity projection operator after the PIRG process. An advantage of QP-PIRG is that much smaller basis sizes $L$ can be used[38].

Following reference 37 we define the energy variance $\Delta E = (\langle \hat{H}^2 \rangle - \langle \hat{H} \rangle^2)/\langle \hat{H} \rangle^2$. $\Delta E$ is used to correct for the finite basis size $L$. For each set of parameters we performed the annealing and A iterations for successively larger basis sizes $L$. Each correlation function was then extrapolated to $\Delta E = 0$ by performing a linear fit. The error bars reported in our results are the standard errors estimated from the linear fit. The largest $L$ used here for 6×6 and 8×8 lattices was 256. The smallest $L$ results we used in the fitting process depended on the value of $U$: for $U \lesssim 2$ we found that even $L$ as small as 4 fit gave a good linear variance extrapolation, while for larger $U$ we only used $L \gtrsim 16$ results in the fit.

In Fig. 2, we compare results from our PIRG code with exact diagonalization results for the 4×4 lattice[10]. Here $L$ of up to 256 were used. Fig. 2(a) shows the variance extrapolation of the energy for $t' = 0.5$. The extrapolated value for ground state energy is -15.037±0.002 compared to the exact ground state of -15.031. In Fig. 2(b) we plot the pair-pair correlation $P_d(r)$ as a function of distance for $U=4$. The inset shows the percent relative error in $P_d(r)$ as a function of $r$. The maximum relative error is for $r = r_{\max}=2\sqrt{2}$ and is smaller than 0.4%. Fig. 2(c) shows the d-wave correlation at the furthest distance, $P_d(r_{\max})$ as a function of $U$ for 4×4, $t' = 0.5$. The inset here shows the variance extrapolation for $P_d(r_{\max})$ for $U=4$. Again, as in Fig. 2(a) the extrapolation of the physical quantity is well within the statistical error.

Our PIRG code was further verified against quantum Monte Carlo (QMC) results for larger lattices in the $t' = 0$ limit where QMC does not suffer from the fermion sign problem at $\frac{1}{2}$-filling. For the $6 \times 6$ lattice, the QMC estimate for the ground state energy[38] of Eq. 1 with $U = 4$ and $t' = 0$ is $E$= -30.87±0.05. Previous QP-PIRG calculations using lattice translations and spin-parity during the PIRG projection process, followed by a total-spin $S = 0$ projection
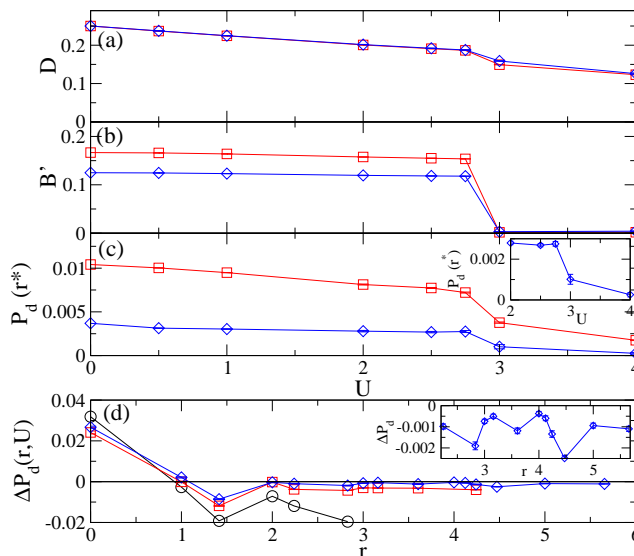
FIG. 3: (color online) PIRG results for t'=0.2. Squares and diamonds are for 6×6 and 8×8 lattices respectively. (a) double occupancy $D$ (b) $t'$ bond orders (c) long distance $d_{x^2-y^2}$ pair-pair correlation function, $P_d(r^\star)$ as a function of $U$ (see text). The inset shows $P_d(r^\star)$ for the 8×8 lattice near the PM-AFM boundary. (d) Enhancement over non-interacting system, $\Delta P_d(r, U)$, for $U = 2.75$ as a function of distance. Circles here are exact $4 \times 4$ results. The inset shows the long-range part of $\Delta P_d(r, U)$ for the 8×8 lattice. In all panels lines are only guides to the eye.

obtained[38] $E=$ -30.879. The extrapolated energy with our choice of $4N$ lattice symmetries, spin-parity projection, and a maximum $L$ of 256 was almost identical, $E=$-30.89±0.04.

## IV. RESULTS

### A. $t' = 0.2$

At $t' = 0.2$ a single transition is expected between PM and AFM phases[3,10]. In Fig. 3(a)-(b) we plot $D$ and $B'$ as a function of $U$. The transition from the PM to an insulating phase is clearly seen as a discontinuous decrease in $B'$ and $D$ at $U = U_c$. $U_c$ is only weakly size dependent at $t' = 0.2$—for the 4×4 lattice[10] $U_c = 2.95 \pm 0.05$, while for $6 \times 6$ and $8 \times 8$ lattices we found 2.75< $U_c$ <3.00. We estimate $U_c \approx 2.7$ in the thermodynamic limit.

For all of the $t'$ values we considered, we found that $d_{x^2-y^2}$ pair-pair correlations were of larger magnitude than $d_{xy}$ correlations (in Section IV C below we show an explicit comparison between the two). Fig. 3(c) shows the $d_{x^2-y^2}$ pair-pair correlations $P_d(r^\star)$ as a function of $U$. The distance $r^\star$ is defined as the next-to-furthest possible separation $r$ between two lattice points on the finite lattice; $r^\star = 2.24, 3.61, 5.00$ for 4×4, 6×6, and 8×8 lattices, respectively. Here we use $r^\star$ rather than the furthest distance $r_{\max}$ because of finite-size effects[45] associated with $r_{\max}$. The 4×4 correlations are considerably larger in magnitude because of the larger $r^\star$ on that lattice and we have not included them on Fig. 3(c). As seen in Fig. 3(c), $P_d(r^\star)$ has a tendency to decrease monotonically with $U$ and is smaller at all nonzero $U$ compared to $U = 0$. At $U_c$ $P_d(r^\star)$ decreases discontinuously.

In addition to the $U$-dependence, it is also important to examine the distance-dependence of pair-pair correlations. In Fig. 3(d) we plot $\Delta P_d(r, U)$, defined as $\Delta P_d(r, U) = P_d(r, U) - P_d(r, U = 0)$, as a function of $r$ for $U$=2.75. Positive $\Delta P_d(r, U)$ indicates enhanced pairing correlations over the noninteracting limit. We choose $U = 2.75$ in the PM state and close to the PM-AFM boundary where the greatest enhancement of pair-pair correlations from AFM fluctuations might be expected from prior work. Fig. 3(d) includes the exact $4 \times 4$ $\Delta P_d(r, U)$ as well. Our results in Figs. 3(c)-(d) show that as the system size increases, the long-range $d_{x^2-y^2}$ pair-pair correlation function approaches that of noninteracting fermions. We have confirmed similar behavior of $\Delta P_d(r, U)$, viz., absence of enhancement for other values of $U$ (not shown here) in either the PM or AFM regions.

As seen in Fig. 3(d), the only enhancement by $U$ in the pairing correlations is at $r = 0$. The $r = 0$ enhancement occurs because $P_d(r = 0)$ contains a component proportional to the nearest-neighbor spin-spin correlation function; the enhancement of AFM order by $U$ leads to an increase[45] in $P_d(r = 0)$. In Fig. 4 we plot $P_d(r = 0)$ as a function of $U$. Precisely at $U_c$ there is a discontinuous *increase* in $P_d(r = 0)$, even as the system becomes *semiconducting*, due to
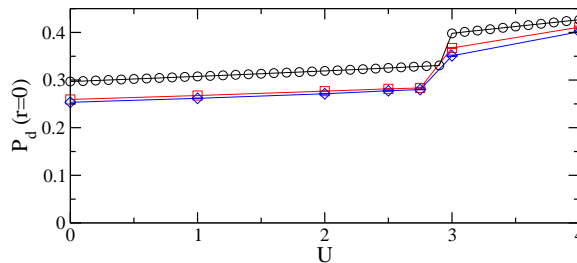
FIG. 4: (color online) Short-distance (see text) $d_{x^2-y^2}$ pair-pair correlation function, $P_d(r=0)$, as a function of $U$ for $t'=0.2$. Circles, squares, and diamonds are for $4 \times 4$, $6 \times 6$, and $8 \times 8$ lattices, respectively. Lines are only guides to the eye.
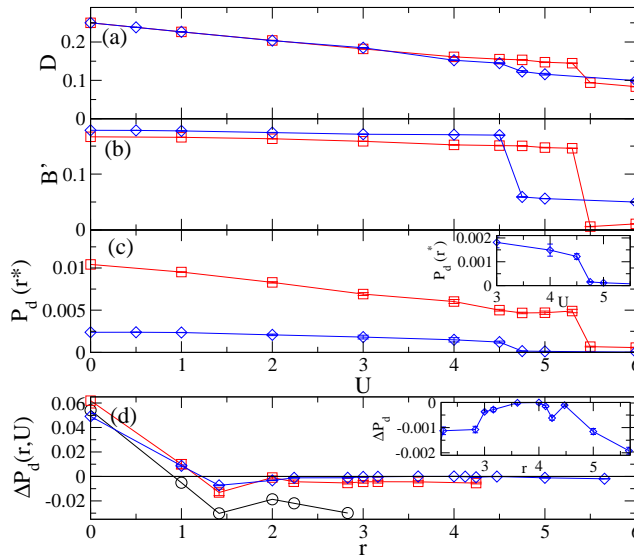


FIG. 5: (color online) PIRG results for $t'=0.5$. Circles, squares and diamonds are for $4\times4$, $6\times6$ and $8\times8$ lattices respectively. Panels (a)–(c) are the same as Fig. 3(a)-(c) except $t'=0.5$. (d) is the same as Fig. 3(d) except $t'=0.5$ and $U=4.5$. In all panels lines are only guides to the eye.

the increase in the magnitude of AFM spin-spin correlations. Importantly, only pair separations of $r > 2$ should be used to judge the enhancement of pairing correlations, because for $r \leq 2$ $d_{x^2-y^2}$ pairs overlap on the lattice[10]. Here we find that $P_d(r)$ for distances beyond nearest-neighbor pair separation always *decrease monotonically with increasing* $U$. As we discuss further in Section V, the spurious increase of short-range correlations is the primary reason that mean-field calculations find SC near the MI transition.

## B.   $t' = 0.5$

Fig. 5 shows $D$, $B'$, and $P_d(r)$ for $t' = 0.5$. Not surprisingly, compared to $t' = 0.2$, $U_{c1}$ depends here more strongly on lattice size, decreasing with increasing system size ($U_{c1} = 5.4 \pm 0.1$ and $4.6 \pm 0.1$ in the $6\times6$ and $8 \times 8$ lattices, respectively). Previous PIRG calculations found $U_{c1} \sim 4.1$ after performing finite-size scaling[3]. Our results are consistent with this value.

In contradiction to $t' = 0.2$ (see Fig. 3(b)), $B'$ here is nonzero on the insulating side of the MI transition, suggesting that the nature of the insulating phase is different. We have also calculated the spin structure factor $S_\sigma(\vec{q})$ (not shown here). For $U > U_{c1}$, a peak appears in $S_\sigma(\vec{q})$ at $\vec{q} = (\pi, \pi)$. However, $S(\pi, \pi)/N$ appears to extrapolate to zero as $N \to \infty$, based on the three lattice sizes we have considered. This indicates that the system does not have long-range AFM order at $t' = 0.5$ for $U > U_{c1}$, consistent with the NMI phase previously identified in this parameter region[2,3]. Note that the larger $B'$ in the NMI phase than in the AFM phase is also consistent with our previous exact diagonalization calculation (see Fig. 2 in Ref. 10.) The properties of the NMI phase and the subsequent NMI-AFM transition at even larger $U_{c2}$ have both been extensively discussed in the literature before[2–4,6,15,16]. Here therefore we focus on the strength of pair-pair correlations as a function of $U$ and distance.
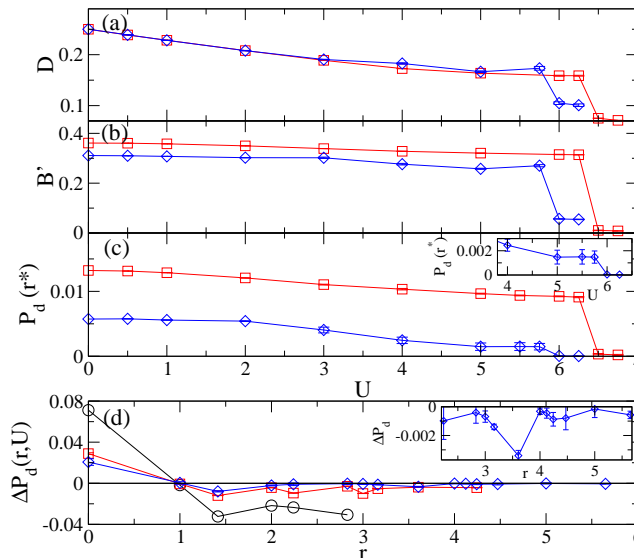
FIG. 6: (color online) PIRG results for $t'=0.8$. Circles, squares and diamonds are for $4\times4$, $6\times6$ and $8\times8$ lattices respectively. Panels (a)-(c) are the same as Fig. 5(a)-(c) except $t'=0.8$. In (d) $t' = 0.8$ and $U = 5.5$. In all panels lines are only guides to the eye.

Fig. 5(c) shows $P_d(r^\star)$ as a function of $U$. As at $t' = 0.2$, $P_d(r^\star)$ decreases monotonically with $U$. At $U = U_{c1}$, $P_d(r^\star)$ decreases discontinuously and is of very small magnitude in the NMI phase. The magnitude of $P_d(r)$ does not increase as $U$ is increased further approaching the AFM phase. Fig. 5(d) shows $\Delta P_d(r, U)$ as a function of distance for $t'=0.5$ for $U=4.5$. As in Fig. 4, at $t' = 0.5$ $P_d(r = 0)$ increases at the MI transition due to the increase in strength of nearest-neighbor AFM correlations, while long distance correlations are again weaker at nonzero $U$ than at $U = 0$.

### C.  $t' = 0.8$

Our results for $t' = 0.8$, shown in Fig. 6, are similar to those for $t' = 0.5$. Here the PM region extends to somewhat larger[3] $U$. As at $t' = 0.2$ and $t' = 0.5$ there is no enhancement of the pairing correlations. $P_d(r = 0)$ again shows an increase at the MI transition. From finite-size scaling we estimated the value for $U_{c1} = 5.0 \pm 0.3$ from our data. This value is identical to earlier results[3].

Several authors have suggested that the symmetry of the superconducting order parameter changes from $d_{x^2-y^2}$ to $d_{xy}$ or $s + d_{xy}$ in the region of the phase diagram close to the isotropic triangular lattice limit[25,30]. In Fig. 7 we compare the $d_{x^2-y^2}$ and $d_{xy}$ correlations for $U = 4$ as a function of $r$. Except at specific small $r$ where pairs can overlap each other on the lattice[10], we find that $d_{x^2-y^2}$ correlations are always stronger than $d_{xy}$ correlations. Plots of the $P_{xy}(\mathbf{r})$ versus $U$ also show a monotonic decrease with increasing $U$, and $\Delta P_{xy}(r, U)$ similarly approaches zero for large $r$.

### V.  DISCUSSION

In Section IV we presented superconducting pair-pair correlations for the ground state of the $\frac{1}{2}$-filled band Hubbard model on the anisotropic triangular lattice calculated using the PIRG method. Our main results are that (i) in all cases the superconducting pair-pair correlations at all finite $U$ are clearly weaker than in the noninteracting limit, except for an enhancement of the very short-range component, and (ii) at large distances the distance dependence of the pair-pair correlations approaches that of the noninteracting system. These results, in conjunction with earlier exact diagonalization results[10], which show exactly the same trends, strongly suggest that the superconductivity is not present in the model. Since many of the earlier works did find SC within the same model Hamiltonian, it is useful to compare these approaches and results with ours. Broadly speaking, two different kinds of methods had predicted SC within the triangular lattice Hubbard model, mean-field and the VMC. We discuss them separately.

*Mean-field approaches:* In all cases, mean-field methods find a superconducting phase *between* the PM and AFM phases[7,8,21,22]. A NMI phase is found by some mean-field methods[7,8,21] but not others[22]. However, there are further
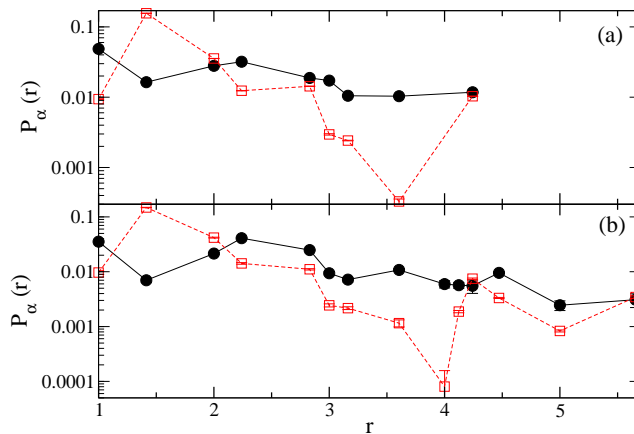
FIG. 7: (color online) Comparison of $d_{x^2-y^2}$ and $d_{xy}$ pair-pair correlations as a function of distance $r$ at $t' = 0.8$ and $U = 4$. (a) 6×6 lattice (b) 8×8 lattice. In both panels, circles (squares) correspond to $\alpha = d$ ($\alpha = d_{xy}$). Lines are only guides to the eye.

inconsistencies—for example, the paramagnetic insulating (PMI) phase in reference 21 in some regions of the phase diagram unrealistically occurs at a temperature *higher* than that of the PM phase. In the NMI phase the nearest-neighbor AFM correlations are strong but AFM long-range order is not present. At fixed $t'$, increasing $U$ drives the system from the PM to NMI phases. Upon entering the NMI the $d_{x^2-y^2}$ correlation at $r = 0$ increases in strength because the $r = 0$ correlation is proportional to the nearest-neighbor spin-spin correlations. Our present results show that *at the same time as this trivial short-range correlation increases, the strength of longer-ranged correlations decrease greatly.* Mean-field methods cannot capture these longer-ranged correlations and erroneously extrapolate from the short-distance limit.

*VMC:* Within VMC a functional form for the wavefunction is assumed at the outset. The three different phases found for intermediate $t'$ (PM, NMI, and AFM) require three different assumptions for the functional form of the wavefunction. This makes determining the true ground state behavior extremely difficult using VMC, especially near the phase boundaries. PIRG uses instead an *unconstrained* superposition of Slater determinants which does not suffer from these problems. The assumption of a functional form is a serious disadvantage as evidenced from the variety of results from different VMC studies which are not consistent with one another. For example, reference 34 did find SC in the model, while a later study by the same authors did not[13]. Liu et al. assume that the wavefunction is a Gutzwiller projected BCS function and find SC[25]. The appropriateness of such a wavefunction to describe SC is however a controversial assumption—Tocchio et al for example did not find SC within the same assumed wavefunction form[15]. The occurrence of the NMI phase within VMC methods seems to be as much of a problem as within mean-field methods—Tocchio et al do not find evidence for NMI at $t'=0.6$ while PIRG does[3,15].

SC has also been found in several models that are closely related to the $\frac{1}{2}$-filled Hubbard model on the anisotropic triangular lattice. These include the Hubbard-Heisenberg model[17,27–31], and the Hubbard model with *two* diagonal $t'$ bonds per square plaquette[26,35]. While we cannot compare directly our PIRG results with these models, in nearly all cases the methods used to study these models are identical to those that have erroneously predicted SC within the present model. We have begun a reinvestigation of these models.

We now return to the superconducting phase found in the organic CTS. Our results here cover the entire parameter region $(0.4 \lesssim t' \lesssim 0.8)$ thought to be appropriate[32,33] for the $\kappa$-phase CTS superconductors within the effective Hubbard model description for them, and clearly indicate that the $\frac{1}{2}$-filled band Hubbard model is not sufficient to explain the occurrence of SC in $\kappa$-ET. It is important in this context to recall that in many CTS superconductors the insulator-superconductor transition is not from an AFM phase but from a different kind of exotic insulator. Examples include $\kappa$-(ET)$_2$Cu$_2$(CN)$_3$, which lacks long-range AFM order even at the lowest temperatures of measurement and has been considered a QSL candidate[1], but is superconducting under pressure[48], and other CTS superconductors where the insulating phase adjacent to superconductivity is nonmagnetic and charge-ordered (CO)[49]. Once again mean-field theory, now within the $\frac{1}{4}$-field band extended Hubbard Hamiltonian on anisotropic triangular lattices has suggested the possibility of a charge fluctuation mediated CO–SC transition[50]. Based on our present work, there are reasons to doubt mean-field approaches to SC within correlated-electron models in general and these earlier results should be checked through many-body calculations.

The different natures of the unconventional semiconductors proximate to SC in the CTS confront theorists with a unique challenge. While mean-field theories suggest a different mechanism for each different semiconductor-

superconductor transition, it appears unlikely to us that structurally similar materials, with identical molecular components in some cases, should require different mechanisms for SC. Given how difficult a problem correlated-electron SC has turned out to be we suggest that an alternate approach is to determine first how to construct a theoretical framework within which a unified theory of SC begins to look feasible, and then to search for the same. We have recently shown how it may be possible to construct such a framework for the CTS[51–54]. In this picture, the $\kappa$-(ET)$_2$X and other dimerized CTS should be described in terms of the *underlying $\frac{1}{4}$-filled band* as with the other CTS superconductors[51,52]. In the presence of strong dimerization and relatively weak frustration, AFM wins. Under increasing frustration though, a transition occurs from AFM with uniform charge density on each dimer to a charge-ordered paired singlet state we have termed the Paired Electron Crystal (PEC)[51,52]. Experimental examples of the PEC in 2D CTS include $\beta$-(*meso*-DMBEDT-TTF)$_2$PF$_6$ (reference 55) and $\beta'$-EtMe$_3$P[Pd(dmit)$_2$]$_2$ (references 56,57), *which have precisely the same CO and bond patterns as in the PEC model[51,52]*, and are superconducting under pressure. The application of pressure corresponds to a further increase in frustration and gives the possibility of a paired electron *liquid* superconductor[58], a realization of the charged boson SC first proposed by Schafroth[59]. Although more work will be necessary to prove this, this theoretical approach has the advantage that it leads to a single model for correlated-electron SC in the CTS. Even more interestingly, we have pointed out that there exist several frustrated strongly correlated *inorganic* $\frac{1}{4}$-filled superconductors that can perhaps be described within the same model[52–54].

Finally, the experimental observation of AFM[60] in expanded fullerides A$_3$C$_{60}$ has led to the modeling of these compounds in terms of a 3D nondegenerate $\frac{1}{2}$-filled band Hubbard model[61]. The threefold degeneracy of the lowest antibonding molecular orbitals in C$_{60}$ is removed by Jahn-Teller instability[60,61]. The observation of a spingap in the antiferromagnetic state validates the nondegenerate description[61]. The dynamic mean-field theory (DMFT) proposed for the AFM to SC transition in the fullerides within this 3D effective $\frac{1}{2}$-filled band Hubbard model[61] is however very similar to the DMFT theories of SC in the 2D CTS[7]. Our results here suggest that a reexamination of the spin-fluctuation mechanism of SC in the fullerides may also be called for.

## VI.   ACKNOWLEDGMENTS

[1] K. Kanoda and R. Kato, Annu. Rev. Condens. Matter Phys. **2**, 167 (2011).

[2] T. Kashima and M. Imada, J. Phys. Soc. Jpn. **70**, 3052 (2001).

[3] H. Morita, S. Watanabe, and M. Imada, J. Phys. Soc. Jpn. **71**, 2109 (2002).

[4] S. Watanabe, J. Phys. Soc. Jpn. **72**, 2042 (2003).

[5] O. Parcollet, G. Biroli, and G. Kotliar, Phys. Rev. Lett. **92**, 226402 (2004).

[6] T. Mizusaki and M. Imada, Phys. Rev. B **74**, 014421 (2006).

[7] B. Kyung and A. M. S. Tremblay, Phys. Rev. Lett. **97**, 046402 (2006).

[8] P. Sahebsara and D. Sénéchal, Phys. Rev. Lett. **97**, 257004 (2006).

[9] T. Koretsune, Y. Motome, and A. Furusaki, J. Phys. Soc. Jpn. **76**, 074719 (2007).

[10] R. T. Clay, H. Li, and S. Mazumdar, Phys. Rev. Lett. **101**, 166403 (2008).

[11] H. Lee, G. Li, and H. Monien, Phys. Rev. B **78**, 205117 (2008).

[12] P. Sahebsara and D. Sénéchal, Phys. Rev. Lett. **100**, 136402 (2008).

[13] T. Watanabe, H. Yokoyama, Y. Tanaka, and J. Inoue, Phys. Rev. B **77**, 214505 (2008).

[14] T. Ohashi, T. Momoi, H. Tsunetsugu, and N. Kawakami, Phys. Rev. Lett. **100**, 076402 (2008).

[15] L. F. Tocchio, A. Parola, C. Gros, and F. Becca, Phys. Rev. B **80**, 064419 (2009).

[16] T. Yoshioka, A. Koga, and N. Kawakami, Phys. Rev. Lett. **103**, 036401 (2009).

[17] S. Guertler, Q. H. Wang, and F. C. Zhang, Phys. Rev. B **79**, 144526 (2009).

[18] A. Liebsch, H. Ishida, and J. Merino, Phys. Rev. B **79**, 195108 (2009).

[19] Z. Q. Yu and L. Yin, Phys. Rev. B **81**, 195122 (2010).

[20] J. Schmalian, Phys. Rev. Lett. **81**, 4232 (1998).

[21] H. Kino and H. Kontani, J. Phys. Soc. Jpn. **67**, 3691 (1998).

[22] H. Kondo and T. Moriya, J. Phys. Soc. Jpn. **67**, 3695 (1998).

[23] M. Vojta and E. Dagotto, Phys. Rev. B **59**, R713 (1999).

[24] G. Baskaran, Phys. Rev. Lett. **90**, 197007 (2003).

[25] J. Liu, J. Schmalian, and N. Trivedi, Phys. Rev. Lett. **94**, 127003 (2005).

[26] A. H. Nevidomskyy, C. Scheiber, D. Sénéchal, and A.-M. S. Tremblay, Phys. Rev. B **77**, 064427 (2008).

[27] J. Y. Gan, Y. Chen, Z. B. Su, and F. C. Zhang, Phys. Rev. Lett. **94**, 067005 (2005).

[28] B. J. Powell and R. H. McKenzie, Phys. Rev. Lett. **94**, 047004 (2005).

[29] J. Y. Gan, Y. Chen, and F. C. Zhang, Phys. Rev. B **74**, 094515 (2006).

[30] B. J. Powell and R. H. McKenzie, Phys. Rev. Lett. **98**, 027005 (2007).

[31] J. G. Rau and H.-Y. Kee, Phys. Rev. Lett. **106**, 056405 (2011).

[32] H. C. Kandpal, I. Opahle, Y.-Z. Zhang, H. O. Jeschke, and R. Valentí, Phys. Rev. Lett. **103**, 067004 (2009).

[33] K. Nakamura, Y. Yoshimoto, T. Kosugi, R. Arita, and M. Imada, J. Phys. Soc. Jpn. **78**, 083710 (2009).

[34] T. Watanabe, H. Yokoyama, Y. Tanaka, and J. Inoue, J. Phys. Soc. Jpn. **75**, 074707 (2006).

[35] H. Yokoyama, M. Ogata, and Y. Tanaka, J. Phys. Soc. Jpn. **75**, 114706 (2006).

[36] M. Imada and T. Kashima, J. Phys. Soc. Jpn. **69**, 2723 (2000).

[37] T. Kashima and M. Imada, J. Phys. Soc. Jpn. **70**, 2287 (2001).

[38] T. Mizusaki and M. Imada, Phys. Rev. B **69**, 125110 (2004).

[39] M. Imada and T. Mizusaki, in *Effective models for low-dimensional strongly-correlated systems*, edited by G. G. Batrouni and D. Poilblanc (AIP Conference Proceedings, New York, 2006), vol. 816, pp. 78–91.

[40] K. Miyagawa, A. Kawamoto, Y. Nakazawa, and K. Kanoda, Phys. Rev. Lett. **75**, 1174 (1995).

[41] K. Miyagawa, A. Kawamoto, and K. Kanoda, Phys. Rev. Lett. **89**, 017003 (2002).

[42] R. T. Scalettar, E. Y. Loh, J. E. Gubernatis, A. Moreo, S. R. White, D. J. Scalapino, R. L. Sugar, and E. Dagotto, Phys. Rev. Lett. **62**, 1407 (1989).

[43] A. Moreo, D. J. Scalapino, and S. R. White, Phys. Rev. B **45**, 7544 (1992).

[44] C. Huscroft and R. T. Scalettar, Phys. Rev. Lett. **81**, 2775 (1998).

[45] T. Aimi and M. Imada, J. Phys. Soc. Jpn. **76**, 113708 (2007).

[46] T. Yoshioka, A. Koga, and N. Kawakami, J. Phys. Soc. Jpn. **77**, 104702 (2008).

[47] T. Yoshioka, A. Koga, and N. Kawakami, Phys. Rev. B **78**, 165113 (2008).

[48] Y. Kurosaki, Y. Shimizu, K. Miyagawa, K. Kanoda, and G. Saito, Phys. Rev. Lett. **95**, 177001 (2005).

[49] M. Dressel, J. Phys.: Condens. Matter **23**, 293201 (2011).

[50] J. Merino and R. H. McKenzie, Phys. Rev. Lett. **87**, 237002 (2001).

[51] H. Li, R. T. Clay, and S. Mazumdar, J. Phys.: Condens. Matter **22**, 272201 (2010).

[52] S. Dayal, R. T. Clay, H. Li, and S. Mazumdar, Phys. Rev. B **83**, 245106 (2011).

[53] S. Mazumdar, and R. T. Clay, Phys. Status Solidi B (2012), in press, corrected proof http://dx.doi.org/10.1002/pssb.201100723.

[54] S. Mazumdar, R. T. Clay, and H. Li, Physica B (2012), in press, corrected proof http://dx.doi.org/10.1016/j.physb.2012.01.016.

[55] S. Kimura, H. Suzuki, T. Maejima, H. Mori, J. Yamaura, T. Kakiuchi, H. Sawa, and H. Moriyama, J. Am. Chem. Soc. **128**, 1456 (2006).

[56] M. Tamura and R. Kato, Sci. Technol. Adv. Mater. **10**, 024304 (2009).

[57] T. Yamamoto, Y. Nakazawa, M. Tamura, A. Nakao, Y. Ikemoto, T. Moriwaki, A. Fukaya, R. Kato, and K. Yakushi, J. Phys. Soc. Jpn. **80**, 123709 (2011).

[58] S. Mazumdar and R. T. Clay, Phys. Rev. B **77**, 180515(R) (2008).

[59] M. R. Schafroth, Phys. Rev. **100**, 463 (1955).

[60] Y. Iwasa and T. Takenobu, J. Phys.: Condens. Matter **15**, R495 (2003).

[61] M. Capone, M. Fabrizio, C. Castellani, and E. Tosatti, Rev. Mod. Phys. **81**, 943 (2009).